JOURNAL OF PROPULSION AND POWER
Vol. 13, No. 4, July–August 1997

Hybrid Friction–Impact Vibration Damper for Cryogenic Rotating Machinery

J. Jeffrey Moore,* Alan B. Palazzolo,† and Ravindera K. Gadangi‡
Texas A&M University, College Station, Texas 77843
and
Alford F. Kascak,§ Gerald Brown,¶ and Gerald Montague**
NASA Lewis Research Center, Cleveland, Ohio 44135

A hybrid friction–impact rotordynamic damper has been designed and tested in a high-speed rotordynamic test rig for application to rocket engine turbopumps operating at cryogenic temperatures, such as the high-pressure oxygen and fuel turbopumps used in the Space Shuttle Main Engines. Test results have shown the impact damper to be effective at larger amplitudes and higher frequencies, whereas the friction damper is effective at lower amplitudes and frequencies. Together, the hybrid damper offers good performance over a wide range of operating conditions. A friction damper design methodology is presented and applied to the experimental test rig.

Nomenclature

C_{eq} = equivalent viscous damping
c = external viscous damping
D = impactor cavity gap
F_k = kinetic friction force
F_s = static friction force
F_0 = forcing function magnitude
k = stiffness of oscillator
m = mass of oscillator
$m_j u_j$ = rotor imbalance at node j
U = vibration amplitude
U_{opt} = optimum amplitude ratio, u_{opt}/D, maximum damping effectiveness
U_{ss} = u_{ss}/D = SS, nondimensional amplitude at resonance
U_0 = nondimensional static displacement $F_0/k/D$
u_{ss} = steady-state amplitude at resonance
X_j, Y_j = rotor node (j) lateral displacement in X, Y direction
x = oscillator mass position
$\boldsymbol{Z}$ = position vector, containing X_j, Y_j, α_j, β_j
z = impactor mass position
α_j, β_j = rotor node (j) angular rotation about Y, X axis
ε = coefficient of restitution
ζ_{eq} = equivalent damping ratio (including contribution of impact and external damping
ζ_{ext} = external viscous damping ratio
μ = mass ratio, impactor mass/oscillator mass
ω = rotational speed, rad/s

Subscripts
$+$ = after impact
$-$ = before impact

Received May 27, 1994; revision received Jan. 12, 1997; accepted for publication March 27, 1997.

*Graduate Research Assistant, Mechanical Engineering Department; currently at Moore Design Services, 909 Water Locust, Bryan, TX 77803.
†Associate Professor, Mechanical Engineering Department.
‡Graduate Research Assistant, Mechanical Engineering Department.
§Senior Research Engineer, U.S. Army.
¶Senior Research Engineer, Dynamics Branch of Structures Group.
**Research Engineer, NYMA.

Introduction

THE purpose of this research is to develop an effective rotordynamic damper for vibration suppression or rocket engine turbopumps operating in a cryogenic environment, such as those used on the Space Shuttle Main Engines (SSMEs). Figure 1 shows a diagram of the SSME turbopump layout. While significant damping has been achieved using interstage damper seals, conventional bearing dampers reliant on the fluid viscosity, such as the squeeze-film type, are not effective because of the low viscosity of the working fluid. Seals obtain much of their damping force as a result of convective fluid dynamics arising from the large pressure drop. Squeeze film dampers, on the other hand, rely heavily on the fluid viscosity to generate damping through viscous shearing. The hybrid friction–impact damper's performance in this study is independent of the working fluid.

An impact damper has been successfully designed and tested in a high-speed rotordynamic test rig and has proven its effectiveness to suppress synchronous vibrations at cryogenic temperatures. Moore et al.[1] show the performance of the impact damper to be a strong function of vibration amplitude, exhibiting both optimum and threshold amplitudes. The threshold amplitude is necessary to initiate damper motion.

An impact damper consists of a secondary (impactor) mass operating in a cavity of a primary (oscillator) mass (see Fig. 2). A clearance exists between the two masses, allowing the impactor to move relative to the oscillator, resulting in periodic impacts. The principle behind impact damping is the removal of vibratory energy through losses that occur during impact in the form of elastic waves, heat, and sound. It is also called a rattle or inertial damper. The impact damper is simple in concept, compact in size, and unlike most viscous dampers, does not require a grounded foundation. These characteristics make the damper relatively easy to retrofit existing designs.

The amount of energy lost upon impact of two bodies is characterized by ε

$$\varepsilon = -[(\dot{z}_+ - \dot{x}_+)/(\dot{z}_- - \dot{x}_-)] \tag{1}$$

which relates the velocities after impact to those before impact. Tests by Radil and Palazzolo[2] have shown that ε is only a weak function of temperature; therefore, little change exists in the performance of an impact damper when operating in a cryogenic environment.

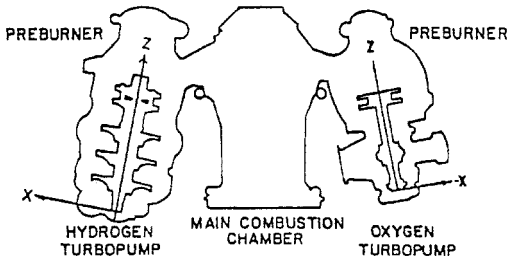

Fig. 1 SSME fuel and oxygen turbopumps.

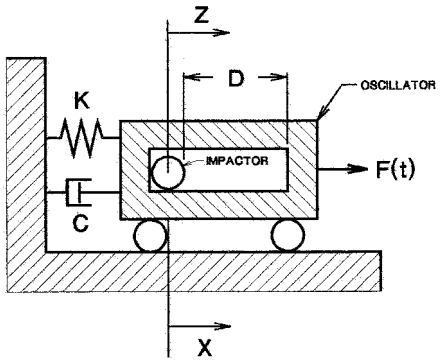

Fig. 2 Single-degree-of-freedom impact damper model.

A novel friction damper has been designed as another viable source of damping at the cryogenic temperatures and differs from previous cryogenic friction dampers in both design and materials. The damping performance of friction damping is inversely proportional to amplitude, making it effective at lower amplitudes. Good performance is obtained at cryogenic temperatures by using a damper design and friction materials that are insensitive to changes in temperature.

Literature Review

Impact dampers have been studied extensively by Masri,[3] Popplewell et al.,[4] Bapat and Sankar,[5] and many others. Most of the early analytical, closed-form solutions to impact damping of a single-degree-of-freedom system assume the impact pattern, namely, the number of impacts per cycle of oscillation. These assumptions limit the results to a finite amplitude range. Recent work by Brown and North[6] show the results of a transient, free-decay, time-history solution of the impact damper by numerically tracking the position of the impactor and oscillator in time to detect impact. New initial conditions may then be determined using the coefficient of restitution principle and conservation of momentum. This approach describes the behavior over a wide amplitude range by defining the following operating regimes: 1) a low-amplitude range with less than one impact per half-cycle of the oscillator and very low damping effect (referred to as impact failure), 2) a medium-amplitude range with a finite number of impacts per half-cycle and good damping characteristics, and 3) a high-amplitude range with an infinite number of impacts per half-cycle (bouncing down to rest on the oscillator wall) and low damping. These conclusions indicate a significant dependence on amplitude for the performance of the impact damper.

Moore et al.[1] applied the method of Brown and North[6] to forced response and studied the effectiveness of an impact damper operating in a cryogenic environment. Moore et al.[1] also performed parametric studies to obtain optimum damper performance. These optimal values compare well with the theory, showing good damping performance over a finite amplitude range.

Friction damping has been used successfully for turbine blade vibration suppression[7] with friction present at the roots, shroud interfaces, and lacing wires. Ku and Heshmat[8] utilize Coulomb friction in bump foil bearings for vibration suppression. Griffin and Menq[9] analytically studied the implications of friction damping of circular vibration control, providing optimal friction magnitudes for a single mass system. Hibner et al.[10] obtained a level of rotor support friction damping equal to the optimal viscous damping in an experimental test rig at room temperature. The friction damping used by Hibner et al.[10] and those used in this study differ by adding damping to the nonrotating bearing housings. Cameron et al.[11] present guidelines for effective friction damping relative to the harmonic excitation force. Similar principles are applied in this paper for rotordynamic systems.

The present work applies the concept of friction damping to supplement the vibration control of impact damping. Furthermore, this investigation describes some unique nonlinear effects friction damping has on the lateral vibration of a flexible rotordynamic system and also shows the effect of stiction on the critical speed response.

Theory

Although the impact damper appears simple, its dynamics can be quite complex because of its highly nonlinear nature during impact. Between separated impacts, the equation of motion for the oscillator is that of a forced harmonic oscillator, and the equation of motion for the impactor is that of a free particle with constant velocity (assuming no friction between the masses) as shown in the following:

$$m\ddot{x} + c\dot{x} + kx = F_0 \cos(\omega t) \tag{2}$$

$$\ddot{z} = 0 \tag{3}$$

where x and z are defined in Fig. 2. The relative velocities before and after impact may be characterized by ε. In addition, linear momentum of the two masses is conserved during impact. These two relations yield the initial conditions after impact for each mass as

$$\dot{x}_+ = \frac{[(1 - \mu\varepsilon)\dot{x}_- + \mu(1 + \varepsilon)\dot{z}_-]}{(1 + \mu)} \tag{4}$$

$$\dot{z}_+ = \dot{x}_+ - \varepsilon(\dot{z}_- - \dot{x}_-) \tag{5}$$

To make the results of the models generally applicable to any single-degree-of-freedom system, the impactor and oscillator's position, velocity, and acceleration are nondimensionalized using the cavity gap D, and time is nondimensionalized using the inverse of the natural frequency (in rad/s):

$$\bar{x} = x/D, \qquad \bar{\dot{x}} = \dot{x}/D, \qquad \bar{\ddot{x}} = \ddot{x}/D \tag{6}$$

$$\bar{z} = z/D, \qquad \bar{\dot{z}} = \dot{z}/D, \qquad \bar{\ddot{z}} = \ddot{z}/D \tag{7}$$

$$\tau = t \cdot \omega_n \tag{8}$$

This solution technique assumes that the time duration of impact is zero, valid for ε greater than 0.5. The equivalent damping ratio is calculated using the following relationship:

$$\zeta_{eq} = \frac{1}{2(U_{ss}/U_0)} \tag{9}$$

The peak U_{ss} is determined for varying static displacements U_0. The equivalent damping ratio includes the contribution of the impact damper plus the added external viscous damping $\zeta_{ext} = 0.01$. Figure 3 shows ζ_{eq} vs U_{ss}. This plot clearly shows the damping effectiveness to be a strong function of amplitude. U_{opt} occurs at 0.379 for this case ($\mu = 0.04$, $\varepsilon = 0.6$). Moore et al.[1] outline a design methodology to optimize impact damper performance.

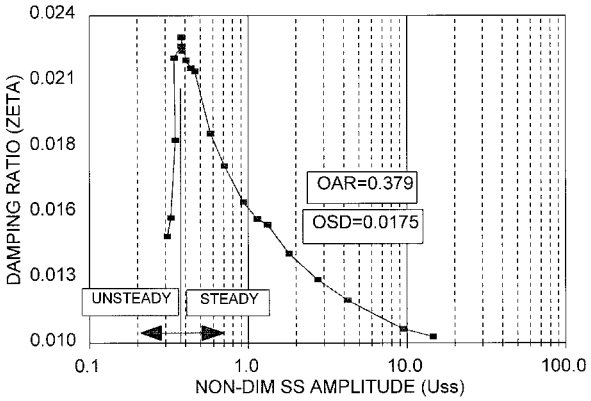

Fig. 3 Damping ratio vs nondimensional amplitude for forced response of SDOF impact damper.

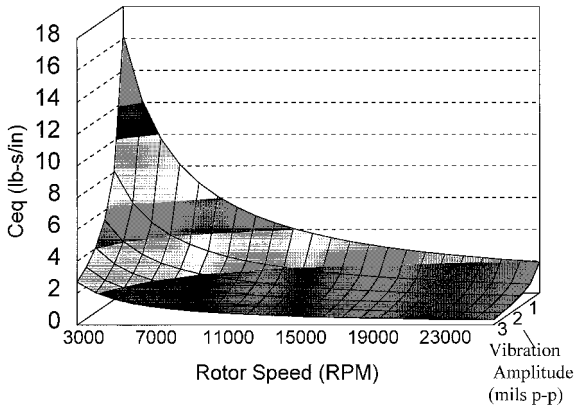

Fig. 4 C_{eq} (lb-s/in.) vs amplitude and speed.

Equivalent viscous damping may also represent Coulomb friction damping by equating the work done per cycle of oscillation to a viscous damper:

$$C_{eq} = 4F_k/\omega\pi U \tag{10}$$

Figure 4 shows C_{eq} (in lb-s/in.) per pound of kinetic friction force for different speeds and vibration amplitudes, and indicates that little friction force is necessary to generate good damping performance, especially at lower speeds and amplitudes. The amount of friction force is limited by the force transmissibility at the bearing support containing the damper, since F_s must be overcome for incipient motion. If F_s is excessive, the damper will lock up and provide no energy dissipation.

Stiction is a measure of the breakaway friction F_s to the sliding friction F_k. Upon incipient motion, the friction force decreases with a given velocity giving rise to a negative damping coefficient. A stick–slip condition may occur that excites the system and is the driver of machine tool chatter and violin strings. Furthermore, since the amount of friction damping that may be added is governed by F_s, high stiction yields relatively low F_k, which lowers damping performance. Previous attempts to add friction damping to a cryogenic rotor system used metal-to-metal contact, which contains high inherent stiction. The design used in this study selects material combinations that minimize stiction.

Friction Damper Design

Friction damper design for high-speed flexible rotors begins first with a rotor model to simulate the rotor flexibility, the bearing coefficients, and the unbalance distribution. A finite element based rotor code is used to discretize the rotor to obtain a system of second-order linear differential equations represented in matrix form by

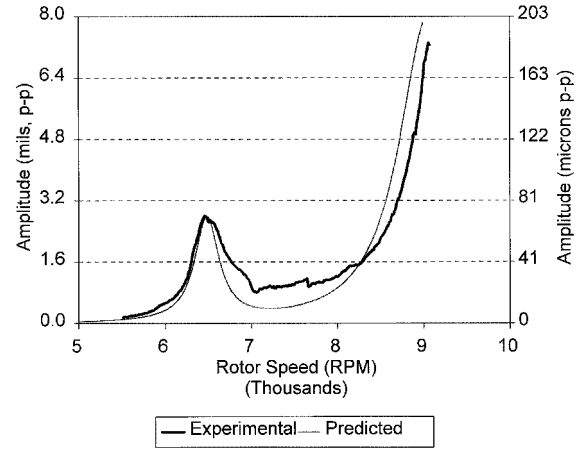

Fig. 5 Frequency response comparison (no damper).

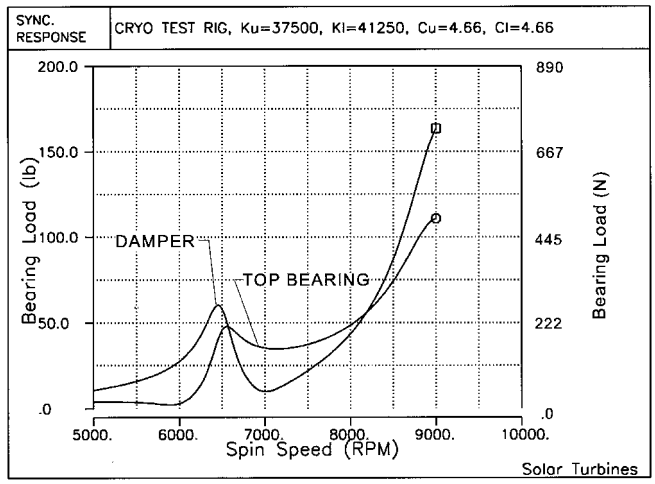

Fig. 6 Calculated bearing force transmissibility (no damper).

$$[M](\ddot{\mathbf{Z}}) + [C](\dot{\mathbf{Z}}) + [K](\mathbf{Z}) = [F(t)] \tag{11}$$

where

$$F_j(t) = m_j u_j \omega^2 e^{i\omega t} \tag{12}$$

This equation is solved for the response at a given speed and unbalance by assuming a harmonic response of the following form:

$$(Z) = (\bar{Z})e^{i\omega t} \tag{13}$$

Solutions of the resulting system of linear, complex equations at multiple speeds generate a frequency response (Bode) plot for each node on the rotor. The rotor model is used to match the experimental response at the two bearings in a high-speed rotor–bearing system (with tare damping only) by adjusting the support coefficients and shaft imbalance. An example is given in Fig. 5 showing the first critical speed at 6450 rpm. Figure 6 gives the calculated bearing force transmissibility for this response using a vectorial sum of the support stiffness and damping forces

$$F_{TR} = U\sqrt{(K_B)^2 + (C_B\omega)^2} \tag{14}$$

where K_B and C_B are the bearing stiffness and damping coefficients, respectively.

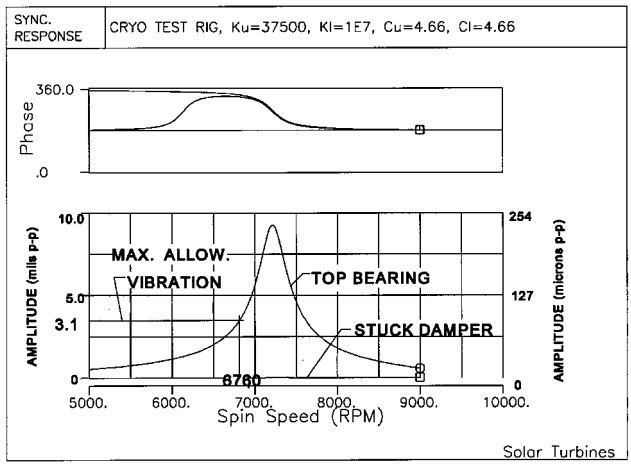

Fig. 7 Calculated frequency response (stuck damper).

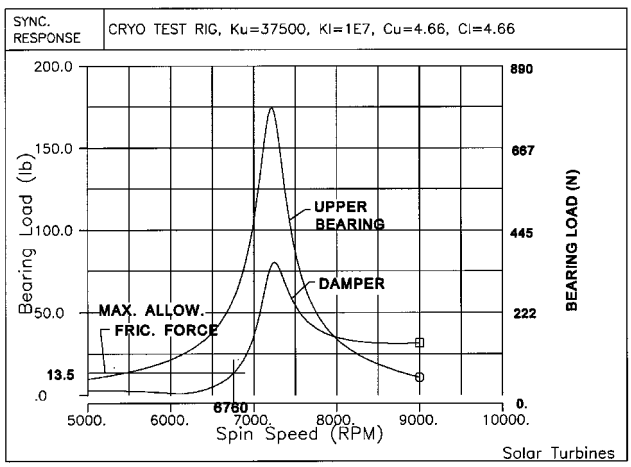

Fig. 8 Calculated bearing force transmissibility (stuck damper).

Once the friction damper is in place at the bottom bearing, no damper motion occurs until the dynamic force exceeds the static friction force. To simulate the condition of a stuck damper, the stiffness is increased to a large value (1.0e7 lb/in., 1.75e9 N/m). The response (Fig. 7) shows larger vibration at the upper bearing and no vibration at the damper. The critical speed has increased to 7200 rpm. Although the stuck damper exhibits no vibration, a dynamic force is still transmitted through the damper and is amplified through the critical speed as shown in Fig. 8. If the damper remains stuck, the vibration and force transmissibility will be worse than with no damper. The amount of friction force allowed is a function of the rotor flexibility, the unbalance magnitude and distribution, as well as the force amplification near the resonance. F_s should be selected so that the damper breaks free at the appropriate amplitude.

Before this friction force may be selected, the maximum allowable vibration at any given point on the rotor must be determined and it defines the speed at which the damper must break free. The dynamic force at the damper corresponding to this speed prescribes the optimum friction force for the system. For example, assume that the maximum allowable vibration at either bearing is 3.1 mil (78.7 μm). With the stuck damper, this vibration level is reached for the top bearing at 6760 rpm (Fig. 7). Figure 8 shows the force transmissibility at the damper to be 13.5 lbf (60.0 N) at this speed, defining the maximum allowable static friction force for this system.

Once the damper breaks free, the stiffness returns to its original value (used in Figs. 4 and 5) as does the critical speed. A speed of 6760 rpm is beyond the no-damper critical speed 6450 rpm. Therefore, the system with the friction damper never encounters the critical speed. Even with no damping contribution, the vibrations are maintained at low levels.

Experimental Setup

The performance of both damper concepts is verified experimentally on a high-speed cryogenic rotor test rig. Figure 9 gives the rotor layout including bearing, sensor, balance plane, and damper locations. The damper assembly operates submerged in a bath of liquid nitrogen (LN_2) at −320°F (−196°C) and speeds up to 18,000 rpm. The critical speeds in the X and Y orthogonal directions are separated for a given mode because of an asymmetric upper bearing housing. Figure 10 shows the hybrid friction–impact damper cross section (left side through friction damper, right side through impactor). The impact damper is mounted in a squirrel-cage fashion and consists of six cylindrical impactors, each operating inside a cylindrical housing. The impactors consist of a dense core, a compliant inner layer, and an outer shell made of a high nickel alloy for good fracture toughness at the low temperatures. Three flats are machined in the outer shell that prevent smooth whirling of the impactors inside their housings. Figure 11 shows a close-up of the impactors and their shell housings.

Six friction dampers are installed in the outer housing (60-deg apart) and dissipate energy through friction between the housing and a hollow push-rod, which follows the radial motion of the squirrel cage (flexible bearing retainer). Figure 12 shows an assembled and exploded view of the friction damper concept. To dampen the small vibration amplitudes, all parts are preloaded using two coil springs. The larger spring preloads a Teflon® friction insert, and its force is varied by the adjustment nut. The smaller spring ensures contact between the push-rod and the squirrel cage. Its preload is changed by installing shim washers between the damper and rotor housings. The friction dampers are skewed 15 deg from the X probe yielding a net contribution of 3.864 times the individual damper friction force in each of the orthogonal directions.

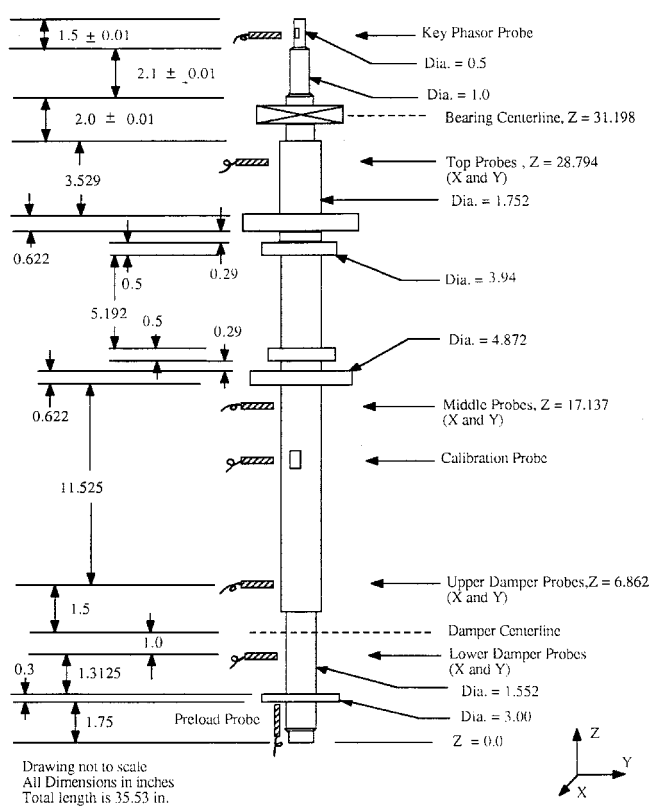

Fig. 9 Rotor shaft with bearing, probe, and balance plane locations.

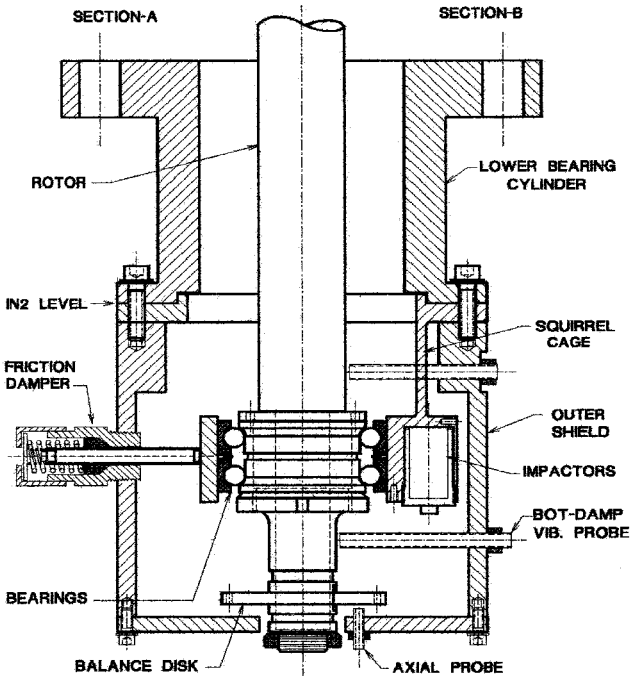

Fig. 10 Hybrid friction–impact damper assembly.

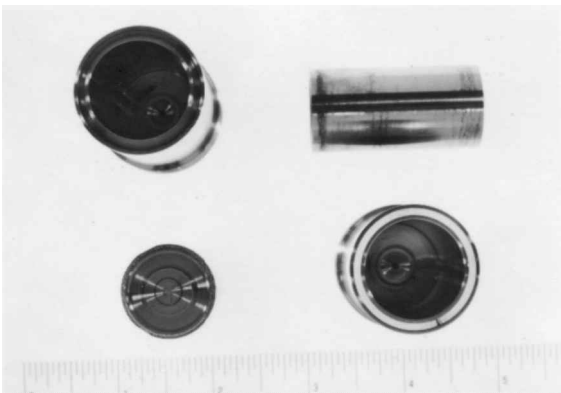

Fig. 11 Close-up of impactor and shell housing.

Fig. 12 Friction damper exploded view.

Teflon (polytetrafluoroethylene, or PTFE) is chosen for the friction material because of its low stiction and ability to accommodate cryogenic temperatures. It has been used successfully as a dry lubricant by impregnating the PTFE into the ball-bearing cages of both the oxygen and hydrogen turbopumps. Because of the relatively low energy associated with the rotor vibratory motion, surface temperatures for both types of dampers are expected to be much less than the 1500 K temperature required for the ignition of the high nickel steel being used.[12] At the highest speed and vibration amplitude during the experimental testing, each friction damper is dissipating energy at a rate less than 1 W.

Table 1 Cryogenic friction study

Friction force	Ambient temperature	Cryogenic temperature
Static	2.0 lbf (8.9 N)	3.5 lbf (15.6 N)
Kinetic	2.0 lbf (8.9 N)	1.8 lbf (8.0 N)

The push-rod is made hollow to lower its inertia, placing the damper's natural frequency well above the maximum rotor speed. The preload springs and segmented friction insert minimize temperature effects on the friction force while cooling to the cryogenic temperatures and also accommodating wear.

To verify the resulting friction force at the cryogenic temperatures, the damper was secured to a plate and dropped into a dewar of LN_2; using a long friction rod, static and kinetic friction values are given in Table 1.

Table 1 shows the stiction increase in the damper at the cryogenic temperature while the kinetic value does not change significantly. Each of the six dampers is set to 2 lbf prior to installation, yielding a net static friction force of 13.5 lbf (3.5 lbf $\times$ 3.864) (60.0 N) and a net kinetic friction force of 6.96 lbf (1.8 lbf $\times$ 3.864) (31.0 N) during the cryogenic operation of the rig. Using Eq. (10), an equivalent viscous damping of 9.4 lb-s/in. (1650 N-s/m) is generated from friction damping at 6000 rpm and 3 mil peak-to-peak (76 μm) of vibration. This is a reasonable level damping for this cryogenic rotor-bearing system.

Test Results

Three different configurations are tested: a) friction and impact dampers, b) friction dampers only, and c) no dampers (baseline). The first two configurations are run with four different unbalance levels. Only the smallest two unbalance sets are possible with the baseline because of vibration limits. These three configurations will be referred to as a, b, and c, respectively, and the imbalance sets will be referred to as 1, 2, 3, and 4, according to Table 2. The weights shown are balance weights, and so removing the weights increases the net unbalance in the shaft. The magnitude and phase are chosen to primarily excite the second mode; however, the first mode is also effected because of its high sensitivity to imbalance.

Balance Weight Set 1

This balance weight set yields the lowest vibration since it cancels residual imbalance. Figures 13a and 13b compare the response of configurations a, b, and c at the lower proximity probe in the X and Y directions for weight set 1. Figure 13a (X probe) shows a dramatic improvement in vibration suppression of the first critical by the friction damper. Notice that the vibration is essentially zero until the damper breaks away at speeds of 6750 and 6800 rpm for configurations a and b, respectively. The breakaway occurred in both X and Y directions simultaneously.

Figure 13b (Y probe) shows the same breakaway speeds. The second Y mode could not be traversed for the baseline because of high vibrations. The friction damper again significantly increased the level of damping in the system allowing passage through the second critical speed. Little difference exists in the response with the impact damper since the vibration is below the threshold amplitude required to initiate impactor motion for the second mode.

Balance Weight Set 2

As the net imbalance is increased, the undamped vibrations grow significantly and prevent the rotor from traversing the

Table 2 Unbalance weight sets

Set number	Plane	Mag, g-mm	ϕ, deg
(1)	Top	242	165
	Mid	185	345
(2)	Top	197	165
	Mid	153	345
(3)	Top	134	165
	Mid	105	345
(4)	Top	65.7	165
	Mid	51.4	345

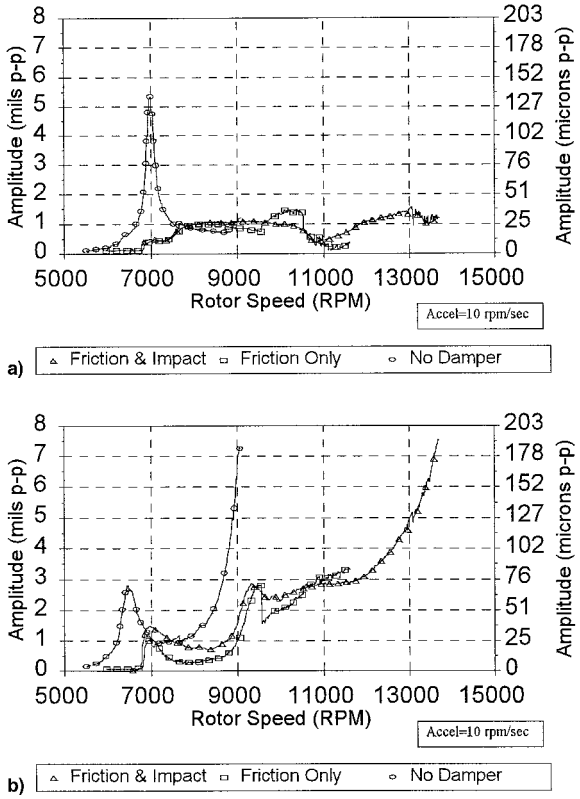

Fig. 13 Rotor response for weight set 1 in a) *X* and b) *Y* directions.

first critical speed in the *X* direction (Fig. 14a). Configurations a and b again produce similar responses and show low sensitivity to imbalance, for both the first and second modes, indicating substantial damping contribution from the friction damper (Figs. 14a and 14b). The breakaway speed drops to 6720 rpm, since the 13.5 lbf (60 N) dynamic force at the damper is reached at a lower speed because of increased imbalance.

Balance Weight Set 3

As the imbalance is further increased, the peak amplitude at the second mode critical speeds increases (Fig. 15). Baseline c data are not acquired at the second critical speed for the larger unbalance sets caused by high vibrations. The damper breakaway decreases again to a speed of 6550 rpm. The response of a and b exhibits similar behavior while traversing the second critical speeds. The impact damper is becoming active for the 2-*X* mode at the larger amplitudes, as indicated by the small-amplitude fluctuations.

Balance Weight Set 4

Figure 16 gives the response for the maximum unbalance level tested. As the amplitude through the second critical speed increases, the friction damping contribution diminishes, yielding a higher amplification factor. With the impact damper added a, the response follows b until a threshold amplitude of 3.5 mil is reached, at which point the impactors become active and effectively limit the amplitude through the critical speed. Moore et al.[1] show that this impact damper configuration possesses optimal performance at a peak amplitude of 4.03 mil (102 μm) and degrades beyond that point. For this case the impact damper is providing most of the damping in the system.

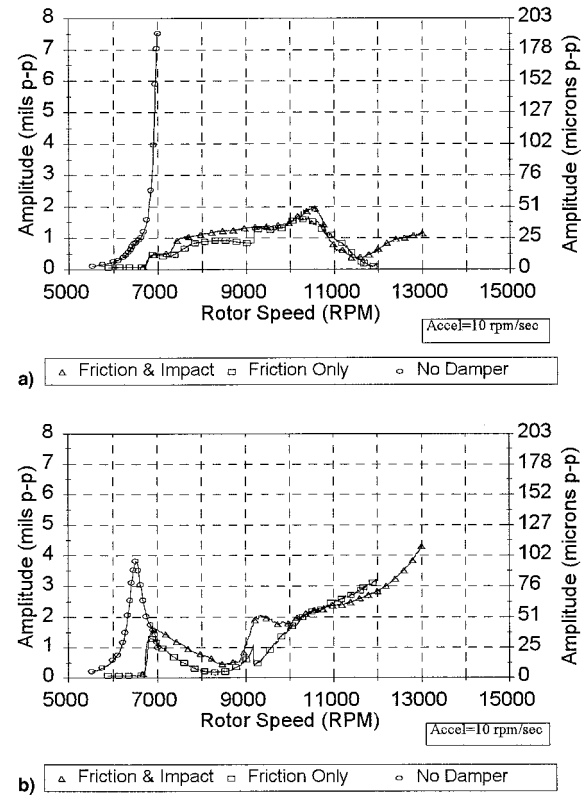

Fig. 14 Rotor response for weight set 2 in a) *X* and b) *Y* directions.

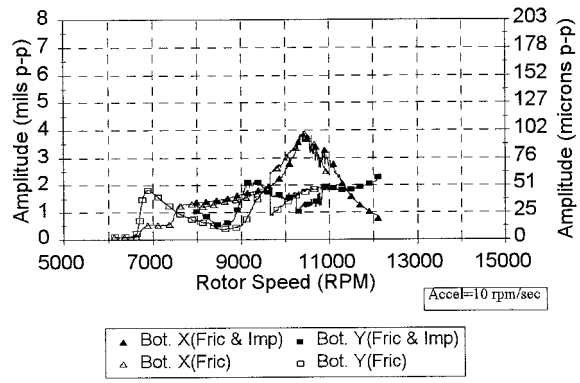

Fig. 15 Rotor response for weight set 3 in *X* and *Y* directions.

Friction Damper Design Applied to Test Rig

The experimental curve in Fig. 5 is the no damper case in Fig. 13b. The calculated breakaway speed of 6760 rpm (F_s = 13.5 lbf) (Fig. 7) agrees quite well with the experimental breakaway speeds of 6750 and 6800 rpm, for configurations a and b, respectively. Therefore, optimal friction damper forces and breakaway speeds for any rotor-bearing system may be calculated using the design methodology previously presented. The breakaway phenomena may also be used as a semiactive damper to avoid a critical speed altogether for systems sensitive to bearing support stiffness.

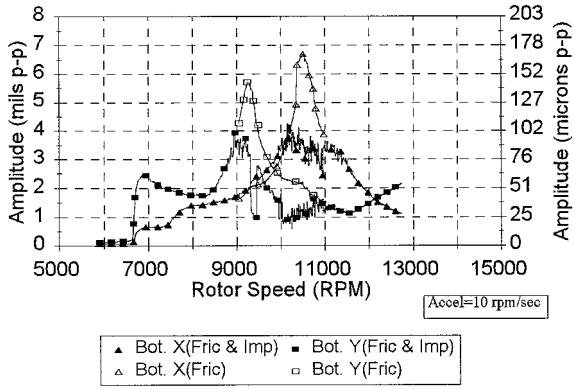

Fig. 16 Rotor response for weight set 4 in *X* and *Y* directions.

Because of its high modal amplitude at the damper, the second mode could benefit from a larger friction force. However, a damper lockup would occur through the first critical causing larger vibrations. Material combinations with lower stiction in the cryogenic environment would provide additional damping with no sacrifice in the breakaway characteristics.

Conclusions

Two rotordynamic shaft dampers, which have been analyzed both analytically and experimentally, yield optimal performance at different vibration amplitudes and speeds. The friction damper yields superior performance at lower amplitudes and speeds. The impact damper requires a given acceleration to initiate impactor motion and, therefore, yields optimal performance for vibration modes with larger amplitudes at the damper and at higher speeds.

The two dampers complement each other providing vibration suppression over the entire speed range; however, careful tuning of the damper parameters is required for each application. The analytical techniques presented have proven to be useful tools in the optimization of each style damper.

Acknowledgments

The authors express their gratitude to NASA's Earth to Space Orbit Propulsion Program for funding this project. Thanks also go to Chester Lee, of Solar Turbines Inc., for providing access to FERDA rotordynamic analysis software.

References

[1]Moore, J. J., Palazzolo, A. B., Gadangi, R. K., Nole, T. A., Klusman, S. A., Brown, G. V., and Kascak, A. F., "A Forced Response Analysis and Application of Impact Dampers to Rotordynamic Vibration Suppression in a Cryogenic Environment," *Journal of Vibrations and Acoustics*, Vol. 117, July 1995, pp. 300–310.

[2]Radil, K., and Palazzolo, A., "The Influence of Temperature and Impact Velocity on Coefficients of Restitution," NASA Memo, 106485, July 1994.

[3]Masri, S. F., "General Motion of Impact Dampers," *Journal of the Acoustical Society of America*, Vol. 47, June 1969, pp. 229–237.

[4]Popplewell, N., Bapat, C. N., and McLachlan, K., "Stable Periodic Vibroimpacts of an Oscillator," *Journal of Sound and Vibration*, Vol. 87, June 1983, pp. 41–59.

[5]Bapat, C. N., and Sankar, S., "Single Unit Impact Damper in Free and Forced Vibration," *Journal of Sound and Vibration*, Vol. 99, No. 1, 1985, pp. 85–94.

[6]Brown, G. V., and North, C. M., "The Impact Damped Harmonic Oscillator in Free Decay," *The Role of Damping in Vibration and Noise Control*, DE-Vol. 5, American Society of Mechanical Engineers, New York, 1987, pp. 53–64.

[7]Rao, J. S., *Turbomachine Blade Vibration*, Wiley, New York, 1991, pp. 7–10.

[8]Ku, R., and Heshmat, H., "Compliant Foil Bearing Structural Stiffness Analysis: Part II: Experimental Investigation," *Journal of Tribology*, Vol. 115, April 1993, pp. 364–369.

[9]Griffin, J. H., and Menq, C. H., "Friction Damping of Circular Motion and Its Implications to Vibration Control," *Journal of Vibration and Acoustics*, Vol. 113, April 1991, pp. 225–229.

[10]Hibner, D. H., Bhat, S. T., and Buono, D. F., "Optimum Friction Damping of a Flexible Rotor," American Society of Mechanical Engineers, 81-GT-156, New York, 1981, pp. 1–5.

[11]Cameron, T. M., Griffin, J. H., Kielb, R. E., and Hoosac, T. M., "An Integrated Approach for Friction Damper Design," *Journal of Vibration and Acoustics*, Vol. 112, April 1990, pp. 175–182.

[12]Bransford, J. W., "Ignition of Metals in High Pressure Oxygen," NASA CP-2372, June 1984, pp. 134–163.